HHS Public Access

Author manuscript

Nature. Author manuscript; available in PMC 2010 December 21.

Published in final edited form as:

Nature. 2010 June 17; 465(7300): 891–896. doi:10.1038/nature09138.

Diphthamide biosynthesis requires an Fe-S enzyme-generated organic radical

Yang Zhang[1,4], **Xuling Zhu**[1,4], **Andrew T. Torelli**[1], **Michael Lee**[2], **Boris Dzikovski**[1], **Rachel M. Koralewski**[1], **Eileen Wang**[1], **Jack Freed**[1], **Carsten Krebs**[2,3], **Steven E. Ealick**[1], and **Hening Lin**[1]

[1]Department of Chemistry and Chemical Biology, Cornell University, Ithaca, NY 14853, USA

[2]Department of Biochemistry and Molecular Biology, The Pennsylvania State University, University Park, Pennsylvania 16802, USA

[3]Department of Chemistry, The Pennsylvania State University, University Park, Pennsylvania 16802, USA

Summary

Archaeal and eukaryotic translation elongation factor 2 contain a unique posttranslationally modified histidine residue called “diphthamide”, the target of diphtheria toxin. The biosynthesis of diphthamide were proposed to involve three steps, with the first step being the formation of a C-C bond between the histidine residue and the 3-amino-3-carboxypropyl group of *S*-adenosylmethionine (SAM). However, details of the biosynthesis have remained unknown. Here we present structural and biochemical evidence showing that the first step of diphthamide biosynthesis in the archaeon *Pyrococcus horikoshii* uses a novel iron-sulfur cluster enzyme, Dph2. Dph2 is a homodimer and each monomer contains a [4Fe-4S] cluster. Biochemical data suggest that unlike the enzymes in the radical SAM superfamily, Dph2 does not form the canonical 5′-deoxyadenosyl radical. Instead, it breaks the $C_{\gamma,Met}$-S bond of SAM and generates a 3-amino-3-carboxylpropyl radical. This work suggests that *Pyrococcus horikoshii* Dph2 represents a novel SAM-dependent [4Fe-4S]-containing enzyme that catalyzes unprecedented chemistry.

Corynebacterium diphtheriae is a pathogenic bacterium that causes the infectious disease diphtheria in humans.[1] This bacterium kills host cells by secreting a protein factor,

Correspondence and requests for materials should be addressed to H.L. (hl379@cornell.edu) or S.E.E. (see3@cornell.edu)..

[4]These authors contributed equally to this work.

Author contributions Y.Z. and X.Z. contributed equally to this work. Y.Z. determined the crystal structure of iron-free *Ph*Dph2, X.Z. performed the biochemical studies and prepared protein samples for spectroscopic and structural studies, A.T. determined the crystal structure of anaerobically purified *Ph*Dph2, M.L. and C.K. performed the Mössbauer spectroscopy, B.D. and J.F. performed the EPR spectroscopy, R.M.K. prepared the initial *Ph*Dph2 crystals, E.W. prepared the *Ph*EF2 mutant proteins, S.E.E. supervised the crystallographic studies, H.L. supervised the biochemical studies. H.L., S.E.E. and C.K. prepared the manuscript.

Author information Atomic coordinates and structure factors for the reported crystal structures have been deposited with the Protein Data Bank under accession codes 3LZC for iron-free *Ph*Dph2 and 3LZD for reconstituted *Ph*Dph2.

Supplementary Information is linked to the online version of this paper at www.nature.com/nature.

Competing interests statement The authors declare no competing financial interests.

diphtheria toxin[2], which catalyzes the ADP-ribosylation of a posttranslationally modified histidine residue (Figure 1) in eukaryotic translation elongation factor 2 (eEF2).[3] Because this posttranslational modification is the target of diphtheria toxin, it was named "diphthamide". eEF2 is a GTPase required for the translocation step of ribosomal protein synthesis.[4] The diphthamide modification is conserved in all eukaryotes and archaea and is important for ribosomal protein synthesis.[4, 5] Although diphthamide was identified more than three decades ago, its biosynthesis has remained an enigma.[6] Five genes required for diphthamide biosynthesis were identified in eukaryotes, *DPH1*, *DPH2*, *DPH3*, *DPH4*, and *DPH5*,[3, 7–13] and a biosynthetic pathway has been proposed (Figure 1).

The first step of diphthamide biosynthesis is the transfer of the 3-amino-3-carboxypropyl (ACP) group from *S*-adenosylmethionine (SAM) to the C-2 position of the imidazole ring of the target histidine residue in eEF2 and is catalyzed by DPH1–4 in eukaryotes. This step is followed by a trimethylation, catalyzed by DPH5, and an amidation, catalyzed by an unidentified enzyme. The first step is particularly interesting for several reasons. First, SAM is generally a methyl donor, but in the first step the ACP group is transferred from SAM. Second, protein posttranslational modifications that involve C-C bond formation are rare[6] and in diphthamide biosynthesis the C-C bond formation involves the poorly nucleophilic C-2 of the imidazole ring. Third, in eukaryotes, this reaction requires four proteins, DPH1–4, raising questions about the function of each protein.

DPH1 and DPH2 share about 20% sequence identity, but are not similar to any other protein with known function. Iterative BLAST searches[14] starting with *Saccharomyces cerevisiae* DPH1 or DPH2 generate both proteins from other eukaryotic species. In contrast, BLAST searches identify only one protein, Dph2, in archaeal species. Archaeal Dph2s are more similar to eukaryotic DPH1 than to DPH2. Eukaryotic DPH3 and DPH4 have no orthologs in archaea based on BLAST searches. To better understand diphthamide biosynthesis, we initially attempted to reconstitute the first step using *Pyrococcus horikoshii* Dph2 (*Ph*Dph2) and translation elongation factor 2 (*Ph*EF2) under aerobic conditions without success. The X-ray crystal structure of *Ph*Dph2 revealed an intriguing constellation of three conserved cysteine residues -- each from a different structural domain -- suggestive of an iron-sulfur cluster. Subsequently, *Ph*Dph2 activity was reconstituted in the presence of dithionite under anaerobic conditions. A crystal structure of reconstituted *Ph*Dph2 along with UV-Vis, EPR, and Mössbauer spectroscopies confirmed the presence of a [4Fe-4S] cluster. Detailed biochemical characterization suggests that the *Ph*Dph2-catalyzed reaction involves a 3-amino-3-carboxypropyl radical intermediate. The data suggest that *Ph*Dph2 is a novel SAM-dependent [4Fe-4S]-containing enzyme[15] that catalyzes unprecedented chemistry.

*Ph*Dph2 is aerobically inactive

*Ph*Dph2 and *Ph*EF2 were expressed in *Escherichia coli* and purified under aerobic conditions. No activity was observed when using these proteins to reconstitute the first step of diphthamide biosynthesis. One explanation for the lack of activity is that the reaction requires an oxygen-sensitive cofactor and another is that additional proteins or small molecules are required. In the latter case the additional proteins might be orthologs of

eukaryotic DPH3 and DPH4; however, attempts to reconstitute activity under similar conditions using yeast DPH1–4 and eEF2 were also unsuccessful (data not shown).

Crystal structure of *Ph*Dph2

To provide structural insight into the catalytic mechanism of *Ph*Dph2, we determined its X-ray crystal structure at 2.3 Å resolution using selenomethionine (SeMet) single anomalous diffraction (SAD) phasing. The structure showed that *Ph*Dph2 is a homodimer (Figure 2). Each *Ph*Dph2 monomer consists of three domains with all three domains sharing the same overall fold. The basic domain fold is a four-stranded parallel β-sheet with three flanking α-helices (or two α-helices and one 3_{10} helix in the case of domain 2) (Supplementary Figure 1). The two β-sheets in domain 1 and 2 each contain an additional β-strand that is antiparallel to the rest of the β-sheet. Domains 2 and 3 have two additional α-helices. Domain 1 of one monomer and domain 3 of the adjacent monomer form the dimer interface, creating an extended nine-stranded β-sheet. The domain folds and their arrangement resemble the structure of quinolinate synthase[16]; however, the orientations of the domains with respect to each other are different in the two enzymes (Supplementary Figure 2). Three conserved cysteine residues (Cys59, Cys163 and Cys287), each coming from a different structural domain, are clustered together in the center of the *Ph*Dph2 monomers. All three cysteine residues are conserved in eukaryotic DPH1s. The first and third cysteine residues are conserved in eukaryotic DPH2s (Supplementary Figure 3).

Reconstitution of *Ph*Dph2 activity

The clustering of the three cysteine residues in the crystal structure and the requirement for SAM raised the possibility that *Ph*Dph2 utilizes a [4Fe-4S] cluster.[15] Radical SAM enzymes harbor a [4Fe-4S] cluster coordinated by three cysteines in a CX_3CX_2C motif[17], although variations of this motif have been reported,[18],[24] to generate a 5′-deoxyadenosyl radical. Since [4Fe-4S] clusters are typically oxygen-sensitive, *Ph*Dph2 was purified and assayed anaerobically. Using ^{14}C-SAM, we showed that *Ph*EF2 can be labeled in the presence of *Ph*Dph2 (Figure 3a, lane 6), but not in the absence of *Ph*Dph2 (lane 3) or dithionite (lane 7). When His600 of *Ph*EF2, the site of the diphthamide modification, was changed to alanine, no reaction occurred in the presence of *Ph*Dph2 (lane 5). MALDI-MS of the *Ph*EF2 protein confirmed that an ACP group was added after the reaction (Figure 3b). These results suggest the possibility that *Ph*Dph2 is a SAM-dependent Fe-S enzyme and demonstrate that no other enzyme is required for the first step of diphthamide biosynthesis *in vitro*.

Characterization of the [4Fe-4S] cluster

The anaerobically purified *Ph*Dph2 contains 1.3 ± 0.2 and 1.9 ± 0.2 equivalents of iron and sulfur per polypeptide, respectively, and displays a broad absorption band at ~400 nm, which disappears upon reduction by 0.5 mM dithionite (Figure 4a). The 400 nm absorption is typical of a $[4Fe\text{-}4S]^{2+}$ cluster. Quantification based on the 400 nm absorption suggests the presence of ~0.3 $[4Fe\text{-}4S]^{2+}$ per *Ph*Dph2. EPR spectra of dithionite-reduced *Ph*Dph2 are shown in Figure 4b. The *g*-values (2.03, 1.92, and 1.86) and the temperature-dependence are typical of a $[4Fe\text{-}4S]^{+}$ cluster.[19]–[22] Quantification of the EPR spectrum suggests the presence of ~0.3 $[4Fe\text{-}4S]^{+}$ per *Ph*Dph2.

The ^{57}Fe-enriched anaerobically-isolated *Ph*Dph2 contains 2.0 ± 0.2 and 2.1 ± 0.2 equivalents of iron and sulfur per polypeptide, respectively. The 4.2-K/53-mT Mössbauer spectrum (Figure 4c) is dominated by a quadrupole doublet with parameters (isomer shift (δ) of 0.43 mm/s and quadrupole splitting parameter (ΔE_Q) of 1.13 mm/s) typical of $[4Fe\text{-}4S]^{2+}$ clusters (solid line in Figure 4c, 73% of total intensity). The weak absorption peak labeled (a) suggests the presence of a small amount (~10%) of high-spin Fe(II), which is presumably nonspecifically bound to the protein. The shoulder labeled (b) belongs to a quadrupole doublet (~15% intensity), the left line of which contributes to the prominent peak at −0.2 mm/s. Although the nature of the Fe species that gives rise to this absorption is not known, similar spectral features were observed for a sample of *P. horikoshii* quinolinate synthase,[23] which is structurally similar to *Ph*Dph2 and also harbors a [4Fe-4S] cluster. Thus, all the spectroscopic data indicate that *Ph*Dph2 contains a [4Fe-4S] cluster.

Brown crystals of the anaerobically purified *Ph*Dph2 were obtained that belong to the same space group as the inactive *Ph*Dph2. A crystal structure determined to 2.1 Å resolution showed clear electron density for a [4Fe-4S] cluster (Figure 4d and Supplementary Figure 4). Refinement of the *Ph*Dph2 structure with a [4Fe-4S] cluster included gave final *R* and R_{free} values of 20.4% and 25.2%, respectively (Supplementary Table 1).

Reaction mechanism

To explore the *Ph*Dph2 reaction mechanism, HPLC was used to analyze the reaction products. In the reaction that contained SAM, *Ph*Dph2, *Ph*EF2 and dithionite, most SAM molecules were converted to 5′-deoxy-5′-methylthioadenosine (MTA, Figure 5a). In control reactions without *Ph*Dph2 or dithionite, only low levels of MTA were observed and most SAM molecules were left intact. This is consistent with the activity assay results shown in Figure 3. Cleavage of the C5′-S bond of SAM did not occur because the formation of 5′-deoxyadenosine (the most likely product of the adenosyl moiety) was not observed. Collectively, the results suggest that *Ph*Dph2 catalyzes the cleavage of the $C_{\gamma,Met}$-S bond of SAM only in the presence of reductant, transfers the ACP group to *Ph*EF2, and releases the remaining MTA.

Two different mechanisms can be proposed for the *Ph*Dph2-catalyzed cleavage of the $C_{\gamma,Met}$-S bond of SAM. One is that the $[4Fe\text{-}4S]^{+}$ cluster provides one electron to reductively cleave the $C_{\gamma,Met}$-S bond of SAM, forming MTA, an ACP radical, and the oxidized $[4Fe\text{-}4S]^{2+}$ cluster (Supplementary Figure 5a). Alternatively, the [4Fe-4S] cluster in *Ph*Dph2 binds SAM and orients it correctly for nucleophilic attack by the C2 of the imidazole ring (Supplementary Figure 5b), leading to the formation of products. Further evidence to differentiate these two possibilities was provided by the identification of the product derived from the ACP group in the reaction without *Ph*EF2. In the absence of *Ph*EF2, *Ph*Dph2 can still cleave the $C_{\gamma,Met}$-S bond of SAM, generating MTA (Figure 5a). The fate of the ACP group was interrogated by ^{1}H-NMR (Figure 5b). In the reaction containing *Ph*Dph2, SAM, and dithionite, several new peaks were observed, which were not observed in control samples without dithionite or *Ph*Dph2 (Figure 5b). These peaks were assigned to two products: 2-aminobutyric acid (ABA) and homocysteine sulfinic acid (HSA). The NMR spectra of authentic samples of ABA and HSA confirmed these

assignments (Figure 5b). In Supplementary Figure 6, these NMR spectra were compared to those of homoserine, homoserine lactone, and SAM, ruling out the possibility that *Ph*Dph2 catalyzes the formation of homoserine or homoserine lactone via a nucleophilic mechanism.

To further validate these results, the reaction mixtures were purified by TLC, dansylated, and subsequently analyzed by LCMS. The structures and molecular weights of the dansylated compounds are shown in Supplementary Figure 7. In the control reaction without *Ph*DPh2, the formation of dansylated homoserine (m/z 337, MH^+, retention time 18.35 min) was observed (Figure 5c and Supplementary Figure 8), which is consistent with the NMR results (Supplementary Figure 6). In the reaction with *Ph*Dph2, SAM, and dithionite, the formation of dansylated homoserine was suppressed compared with the control. Instead, dansylated ABA (*m*/*z* 337, MH^+, 23.60 min) and HSA (*m*/*z* 401, MH^+, 16.65 min) were observed (Figure 5c and Supplementary Figure 8). Dansylated homoserine lactone and ABA have the same retention time, but can be differentiated by their *m*/*z*-values (337 and 335 for ABA and homoserine lactone, respectively, Supplementary Figure 9). During the TLC purification and dansylation reaction, HSA was partially oxidized to homocysteine sulfonic acid, as evidenced by the ion with *m*/*z* 417 (MH^+, Figure 5c and Supplementary Figure 8). Overall, the results from the LCMS analysis and NMR analysis demonstrate that *Ph*Dph2 catalyzes the formation of ABA and HAS in the absence of *Ph*EF2. The formation of ABA and HSA can be best explained by the generation of an ACP radical followed by hydrogen extraction to give ABA or quenching by dithionite to give HSA (Figure 6).

Discussion

The biochemical, structural and spectroscopic data presented here establish that *Ph*Dph2 is a novel [4Fe-4S] cluster enzyme. *Ph*Dph2 cleaves the $C_{\gamma,Met}$-S bond of SAM to MTA and transfers the ACP group to His600 of *Ph*EF2. This reaction is strictly dependent on the presence of reductant. In the absence of the natural substrate, *Ph*EF2, the ACP moiety is trapped either as ABA or as HSA, which suggests the intermediacy of an ACP radical. The reductive cleavage of SAM to a thioether and an alkyl radical by a reduced $[4Fe\text{-}4S]^+$ cluster is the hallmark feature of the superfamily of radical SAM enzymes.[15] However, there are two crucial differences between the radical SAM enzymes and *Ph*Dph2. First, the radical SAM enzymes exclusively cleave the C5′-S bond to generate methionine and a 5′-deoxyadenosyl radical, which is used for a variety of downstream C-H cleavage reactions. Second, the radical SAM superfamily is characterized by a conserved CX_3CX_2C motif[17] (or CX_2CX_4C in ThiC[18], or CX_5CX_2C in HmdA[24]) that binds the [4Fe-4S] cluster. This motif is not present in *Ph*Dph2. Instead the three conserved cysteine residues are located in separate structural domains and are separated by more than 100 residues in the sequence. Consequently, the three-dimensional structure of *Ph*Dph2 is distinct from the structures of the known radical SAM enzymes BioB,[25] HemN,[26] LAM,[27] MoaA,[28] PFL-AE,[29] and ThiC[18], which all have β-barrel or modified β-barrel folds. *Ph*Dph2 is structurally similar to quinolinate synthase,[16] which is also composed of three structurally homologous domains in a triangular arrangement. The triangular arrangement of domains in *Ph*Dph2 positions the three conserved cysteine residues in the central cavity to bind the [4Fe-4S] cluster. In quinolinate synthase, the three conserved cysteine residues required to bind the cluster are also widely separated in the amino acid sequence and located in different domains.[30,22]

However, quinolinate synthase is not SAM-dependent and its proposed role is in the dehydration of the penultimate precursor of quinolinate.[22] In addition, the IspH enzyme in the non-mevalonate pathway for isoprenoid biosynthesis also uses a similar triangular arrangement to bind a [3Fe-4S] cluster.[31]

It is likely that the different reaction outcome, i.e. cleavage of the C5′-S bond in the radical SAM enzymes vs. cleavage of the $C_{\gamma,Met}$-S bond in *Ph*Dph2, is controlled by different orientations of SAM relative to the [4Fe-4S] cluster. In the radical SAM enzymes, the amino and carboxyl groups of SAM coordinate to the non-cysteine-ligated Fe site of the [4Fe-4S] cluster.[32] Future structural and spectroscopic studies are required to investigate how SAM is bound at the active site of *Ph*Dph2.

Our data demonstrated that *Ph*Dph2 is the only gene product required to catalyze the first step of diphthamide biosynthesis *in vitro*. In contrast, biosynthesis of diphthamide in eukaryotes requires four gene products, DPH1–4. Studies on *Ph*Dph2 provide important insight into the functions of eukaryotic DPH1–4. The crystal structure shows that *Ph*Dph2 is a homodimer. Eukaryotic DPH1 and DPH2 are both homologous to each other and to archaeal Dph2. In addition, DPH1 and DPH2 in eukaryotes form a heterodimer.[3, 33–35] Therefore it is possible that the eukaryotic DPH1–DPH2 heterodimer is structurally homologous to the *Ph*Dph2 homodimer. The three cysteine residues required to bind the cluster are conserved in DPH1 and two of the cysteine residues are conserved in DPH2. Thus the heterodimer of DPH1–DPH2 should at least bind one [4Fe-4S] cluster and may be sufficient to catalyze the first step *in vitro*. DPH2, which only has two of the conserved Cys residues, could either have a different catalytic function than DPH1 or could be regulatory. *In vivo*, DPH3 and DPH4 are also required for diphthamide biosynthesis.[3] These gene products may be required to keep the [4Fe-4S] cluster in a reduced state. This hypothesis is supported by the observation that DPH3 can bind iron and is redox active.[36] Alternatively DPH3 and DPH4 may be required for proper assembly of the [4Fe-4S] clusters. The Fe-S cluster assembly pathways in bacteria and mitochondria of eukaryotes are known to involve J domain-containing co-chaperone proteins, such as bacterial HscB and yeast JAC1[37, 38], that are similar to DPH4. Confirmation of these functional assignments awaits detailed biochemical and structural studies.

METHODS SUMMARY

Crystallization, data collection, and structure determination

SeMet *Ph*Dph2 and anaerobically reconstituted *Ph*Dph2 were crystallized using the hanging drop vapor diffusion method. The X-ray data were collected at the NE-CAT beamlines at the Advanced Photon Source (APS). The structures of iron-free *Ph*Dph2 and reconstituted *Ph*Dph2 were determined by SeMet SAD phasing and the Fourier synthesis, respectively.

Reconstitution of activity

Reconstituted *Ph*Dph2 was prepared by growing cells in LB media supplemented with $FeCl_3$, $Fe(NH_4)_2(SO_4)_2$, and L-Cys, and purified using Ni-NTA affinity chromatography anaerobically. The reaction was monitored using carboxyl-^{14}C SAM.

Analysis of reaction products

The formation of MTA was detected by HPLC. Modification of *Ph*EF2 His600 was confirmed by MALDI-MS after trypsin digestion. The products derived from the ACP group were detected by NMR directly and by LCMS after dansylation.

EPR and Mössbauer spectroscopy

ESR spectra were recorded on a Bruker EMX spectrometer at a frequency of 9.24 GHz under standard conditions. Mössbauer spectra were recorded on a spectrometer from WEB research (Edina, MN) operating in the constant acceleration mode in transmission geometry.

Full Methods and any associated references are available in the online version of the paper at www.nature.com/nature.

Methods

Cloning, expression and purification of *Ph*Dph2 under anaerobic conditions

The gene encoding *P. horikoshii* Dph2 was amplified by PCR from *Pyrococcus horikoshii* genomic DNA and inserted into pENTR™/TEV/D-TOPO® entry vector (Invitrogen), followed by recombination with pDESTF1 destination vector to create expression clones with an N-terminal His_6 tag. The plasmids were transformed into the *E. coli* expression strain BL21(DE3) with pRARE. The cells were grown in LB media with 100 μg/ml ampicillin at 37 °C and were supplemented with $FeCl_3$, $Fe(NH_4)_2(SO_4)_2$ and L-cysteine to final concentrations of 50 μM, 50 μM and 400 μM, respectively, when the absorbance of the cell culture reached an OD_{600} of 0.8. The cells were induced at an OD_{600} of 0.8 – 1.0 with 0.1 mM isopropyl-β-D-thiogalactopyranoside (IPTG), at which point the culture flasks were sealed to limit the amount of oxygen in the system. The induced cells were incubated in a shaker (New Brunswick Scientific Excella E25) at 37 °C and 200 rpm for 3 h before being transferred to the 4 °C cold room, where they were kept overnight without agitation. Cells were harvested the second day by centrifugation at 6,371 g (Beckman Coulter Avanti J-E), 4 °C for 10 min. Purification of *Ph*Dph2 was performed in an anaerobic chamber (Coy Laboratory Products) except for the centrifugation step. Cell pellets (from 2 l LB culture) were re-suspended in 30 mL lysis buffer (500 mM NaCl, 10 mM $MgCl_2$, 5 mM imidazole, 1 mM DTT and 20 mM Tris-HCl at pH 7.4). Cells were lysed by incubating with 0.3% (w/v) lysozyme (Fisher) at 26 °C for 1 h, followed by freezing in liquid nitrogen and thawing at 26 °C once. Cell debris was removed by centrifugation at 48,384 g (Beckman Coulter Avanti J-E) for 30 min. The supernatant was incubated for 1 h with 1.2 ml Ni-NTA resin (Invitrogen) pre-equilibrated with the lysis buffer. The resin after incubation was loaded onto a polypropylene column and washed with 20 ml lysis buffer. *Ph*Dph2 was eluted from the column with elution buffers (100 mM or 150 mM imidazole in the lysis buffer, 3 ml each). The brown-colored elution fractions were buffer exchanged to 150 mM NaCl, 1 mM DTT, and 200 mM Tris-HCl at pH 7.4 using a Bio-Rad 10–DG desalting column. The protein was further purified by heating at 95 °C for 10 min and centrifugation at 48,384 g to remove the precipitate. Purified *Ph*Dph2 was concentrated using Amicon Ultra-4 centrifugal filter devices (Millipore).

Expression and purification of SeMet substituted *Ph*Dph2

*Ph*Dph2.pDESTF1 was transformed into the methionine-auxotrophic *E. coli* strain B834(DE3) pRARE that was obtained by transforming pRARE plasmid into B834(DE3). Cells were grown in M9 minimal medium supplemented with all amino acids (0.04 mg/mL) except L-methionine, 50 mg/l L-SeMet, 1× MEM vitamin solution, 0.4% (w/v) glucose, 2 mM $MgSO_4$, 25 mg/ml $FeSO_4$ and 0.1 mM $CaCl_2$. The SeMet substituted *Ph*Dph2 was overexpressed and purified similarly as described above except aerobically and no additional iron and cysteine were added to the media.

Expression and purification of ^{57}Fe-labeled *Ph*Dph2 for Mössbauer spectroscopy

E. coli BL21pRARE cells transformed with *Ph*Dph2.pDESTF1 were grown in M9 minimal medium supplemented with 0.2% (w/v) glucose, 2 mM $MgSO_4$ and 0.1 mM $CaCl_2$ at 37 °C. The ^{57}Fe stock solution was prepared by dissolving ^{57}Fe powder (Isoflex USA) in HCl to final concentrations of 1 M iron and 2.5 M chloride. The ^{57}Fe stock solution and L-Cys were added to M9 media to final concentrations of 100 μM and 400 μM, respectively, before induction. The cells were induced at an OD_{600} of 0.8 with 100 μM IPTG and incubated at 20 °C for an additional 20 h. ^{57}Fe labeled *Ph*Dph2 was anaerobically purified by following the same procedure used for the native protein purification. The final protein concentration, determined by Bradford protein assay (Bio-Rad), was 30 mg/ml (~800 μM). Iron was quantified by using the commercial Quantichrom iron assay kit (DIFE-250, Bioassay systems).

Cloning, expression and purification of *Ph*EF2

Cloning of *Ph*EF2 followed the same protocol as that of *Ph*Dph2. The plasmid was transformed into the *E. coli* expression strain, BL21 (DE3) with a pRARE plasmid. The cells were grown in LB media at 37 °C and induced at an OD_{600} of 1.0 with 0.1 mM IPTG. Cells were harvested after 3 h of induction by centrifugation at 6,000 rpm for 10 min. *Ph*EF2 was purified through Ni-NTA affinity chromatography following the same protocol for *Ph*Dph2. The protein was further purified by heating at 95 °C for 10 min and subsequent FPLC purification using a Superdex 200 gel filtration column and a Q6 anion exchange column (Bio-Rad).

Anaerobic reconstitution of *Ph*Dph2 activity and mass characterization of *Ph*EF2

The reaction components, 12 μM *Ph*EF2, 24 μM *Ph*Dph2, and 10 mM dithionite were added to 150 mM NaCl, 1 mM DTT, and 200 mM Tris-HCl at pH 7.4 to a final volume of 15 μl in the anaerobic chamber under strictly anaerobic conditions. The reaction vials were sealed before taking out of the anaerobic chamber. ^{14}C-SAM (2μL, final concentration of 267 μM) was injected into each reaction vial to start the reaction. The reaction mixtures were vortexed briefly to mix and incubated at 65 °C for 40 min. The reaction was stopped by adding protein loading dye to the reaction mixture and subsequent heating at 100 °C for 10 min, followed by 12% SDS-PAGE electrophoresis. The dried gel was exposed to a PhosphorImaging screen (GE Healthcare, Piscataway, NJ) and the radioactivity was detected using a STORM860 phosphorimager (GE Healthcare, Piscataway, NJ).

Enzymatic reactions with normal SAM followed the same procedure, except that normal SAM was introduced in the anaerobic chamber. The *Ph*EF2 band from the Coomassie blue-stained SDS-PAGE gel was cut out and digested by trypsin. Digestion products were extracted and cleaned using a Millipore Ziptip C4, then characterized by MALDI-MS at the Proteomics and Mass Spectrometry Facility of Cornell University.

Analysis of reaction products with HPLC

Under anaerobic conditions, reactions were set up that contained 30 μM *Ph*EF2, 30 μM *Ph*Dph2, 10 mM dithionite, 31 μM SAM, 150 mM NaCl, 1 mM DTT, and 200 mM Tris-HCl at pH 7.4 in a final volume of 64 μl. The mixture was incubated at 65 °C for 5 min, and then frozen at −20 °C. The reaction mixture was ice-thawed and TFA was added to a final concentration of 5%, followed by centrifugation to separate the precipitated proteins and the supernatant. The precipitated proteins were re-dissolved and *Ph*EF2 was checked by MALDI-MS as described above to make sure the reaction had occurred. The supernatant was analyzed by HPLC (Shimadzu) on a C18 column (HαSprite) monitored at 260 nm absorbance, using a linear gradient from 0 to 40% buffer B in 20 min at a flow rate of 0.3 ml min^{-1} (buffer A: 50 mM ammonium acetate, pH 5.4; buffer B, 50% (v/v) methanol/water).

^{1}H NMR of reaction mixture

A complete reaction (260 μM *Ph*Dph2, 10 mM dithionite and 1000 μM SAM, in 1 ml of 100 mM phosphate buffer with 150 mM sodium chloride, pH=7.4) and control (without *Ph*Dph2 or without dithionite) were set up anaerobically. After incubation at 65 °C for 40 min, *Ph*DPh2 was removed using a Millipore YM-10 Microcon filter unit. The flow-through was lyophilized overnight to dryness and then dissolved in 300 μL D_2O for NMR. Shigemi D_2O matched NMR tube was used. ^{1}H NMR spectra were obtained on an INOVA 400 spectrometer. Compared with controls, four new peaks were identified on ^{1}H NMR: *a*. 0.95 ppm (t, 1H, J = 7.6 Hz), *b*. 1.88 ppm (m, 1H), *c*. 2.12 ppm (m, 2H) and *d*. 2.43 ppm (t, 1H, J = 7.5 Hz). H-H DQCOSY 2D NMR spectrum (data not shown) showed that peak *a* is coupled to b, peak c is coupled to d and another peak (3.78 ppm) that is hidden under the huge signal from buffer. NMR data were analyzed by MestReNova (version 6.0.1).

Dansylation reaction to detect the MS of the reaction products by LC-MS

NMR samples were desalted and purified by TLC silica gel $60F_{254}$ (EMD Chemicals Inc.) with developing solvent (n-butanol : acetic acid : water = 2:1:1). The desired product bands (Rf 0.15 –0.65, below the Rf value of 5′-deoxy-5′-methylthioadenosine) were cut off the TLC plates and the products were washed off the silica gel by water and lyophilized overnight to dryness. The lyophilized products were dissolved with 50 mM sodium bicarbonate to a final concentration approximately 5 times of that of the NMR reaction. The solution was adjusted to pH 9–10 by 12% NaOH. Dansylation reactions were initiated by adding 0.5 volume of 50 mM dansyl chloride in acetonitrile to the solution and the reactions were carried out at room temperature in the dark for 30 min. Dansylated products were separated and analyzed by LC-MS with a linear gradient 0–80% solvent B in 33 min, at a flow rate of 0.8 ml/min. LC-MS experiments were carried out on a SHIMADZU LCMS-QP8000α with C18 column (250 × 4.6 mm, 10 μm, Grace Davison Discovery Sciences

Headquarters) monitoring at 254 and 335 nm with positive mode for mass detection. Solvents for LC-MS were water with 0.1% formic acid (solvent A) and acetonitrile with 0.1% formic acid (solvent B).

Sample preparation for Mössbauer spectroscopy and EPR

Anaerobically purified ^{57}Fe-labeled *Ph*Dph2 was dialyzed into a buffer containing 200 mM Tris-HCl (pH 7.4), 150 mM NaCl, 1 mM DTT and 10% glycerol, and concentrated to 25 – 30 mg/mL. The sample was frozen in liquid nitrogen in the anaerobic chamber for Mössbauer spectroscopy.

For EPR measurements, *Ph*Dph2 (700 μM, with 15% glycerol) with and without 16 mM dithionite were incubated for 30 min before loading into an EPR quartz tube in the glovebox.

Crystallization and structure determination of iron-free *Ph*Dph2

Aerobically purified iron-free *Ph*Dph2 proteins were dialyzed to 10 mM sodium acetate at pH 4.6 and concentrated to 12 mg/ml for the crystallization experiments. The native protein was subjected to a series of sparse matrix screens (Hampton Research, Emerald Biostructures) using the hanging drop vapor-diffusion method at 18 °C in order to determine initial crystallization conditions. Best crystals for both SeMet substituted and native *Ph*Dph2 were obtained from 6 – 8% PEG 4000, 0.1 M ammonium acetate, 0.2 M KCl, 2% ethylene glycol, and 0.05 M sodium citrate at pH 5.1 – 5.3. These crystals belong to the space group $P2_12_12_1$ with typical unit cell dimensions of a = 58.5 Å, b = 82.0, and c = 160.0 Å. Each asymmetric unit contains two monomers, corresponding to a solvent content of 50.3% and Matthews coefficient of 2.47 Å^3/Da.

The *Ph*Dph2 SeMet crystals were briefly transferred into a solution containing 6% glycerol, 16% ethylene glycol, 10% PEG 4000, 0.2 M ammonium acetate, 0.2 M KCl, and 0.1 M sodium citrate at pH 5.3 for cryoprotection. The crystals were allowed to soak in the cryo-solution for 30 – 45 s before plunging them into liquid nitrogen. In an attempt to reconstitute the iron sulfur clusters in crystals, native crystals were soaked in 10% PEG 4000, 100 mM citrate pH 5.3, 200 mM ammonium acetate, 200 mM KCl, 10% ethylene glycol, 8 mM SAM, 4 mM $Fe(NH_4)_2(SO_4)_2$, 4 mM NaS, and 40 mM DTT for 1 h prior to the same cryoprotection and freezing procedure described above.

Data sets were collected at the Advanced Photon Source beamlines 24-ID-C and 24-ID-E using ADSC Quantum 315 CCD detectors. For the single wavelength SeMet data set, the energy was selected to maximize Δf” of the incorporated selenium (12661.5 eV, 0.97922 Å). Data sets were integrated and scaled using HKL2000[39]. Data processing statistics are summarized in Supplementary Table 1.

Eight selenium atom positions were determined using HKL2MAP[40]. These sites were used for SAD phasing using MLPHARE[41] at 2.5 Å resolution. Initial phases were further improved through density modification, twofold noncrystallographic symmetry averaging, and phase extension for the 2.3 Å resolution native data using RESOLVE.[42], [43] The resulting map was readily interpretable and an initial model was built using the interactive

graphics program Coot[44]. The model refinement was carried out through alternating cycles of manually rebuilding using Coot, restrained refinement and water picking using Refmac5[45] and Phenix[46]. Structure refinement statistics are summarized in Supplementary Table 1.

Crystallization and structure determination of reconstituted *Ph*Dph2

Reconstituted *Ph*Dph2 protein was dialyzed to 100 mM NaCl, 1 mM DTT, and 10 mM sodium acetate at pH 4.6, concentrated to 20 mg/ml, and crystallized anaerobically at 26 °C in the glove box using the hanging drop vapor diffusion method. Anoxic sparse matrix screening solutions (Hampton Research, Emerald Biostructures) were used for initial crystallization screens. The optimized crystallization condition is as follows: drops were set up with 1.3 μl protein and an equal volume of 25 – 30% PEG 400, 0.2 M lithium sulfate and 0.1 M MES at pH 6.5, and were equilibrated against a reservoir solution of 0.6 M lithium chloride. Crystals appeared in a week and belonged to the same space group as that of the iron-free structure ($P2_12_12_1$ with averaged unit cell dimensions of a = 55.7 Å, b = 80.5 Å and c = 162.1 Å). Prior to the data collection experiment, crystals were cryoprotected with 2.5 – 5% ethylene glycol, 25 – 30% PEG 400, 0.2 M lithium sulfate, and 0.1 M MES at pH 6.5, then plunged directly into liquid nitrogen in the glove box. A total of 200° of data were recorded at an energy of 12662.0 eV on an ADSC Quantum 315 CCD detector. The data were integrated and scaled to 2.1 Å resolution using HKL2000[39]. The previously solved structure of *Ph*Dph2 lacking the iron sulfur cluster was used to generate phases by Fourier synthesis. A difference Fourier map was calculated and averaged for the two monomers to improve the electron density, and the resulting map was used to model the [4Fe-4S] cluster. A 2.8 Å resolution anomalous difference Fourier map calculated from a data set collected at 7150 eV (1.73405 Å) was also used as a reference for positioning the [4Fe-4S] cluster (not shown). The structure was refined using CNS[47]. X-ray experiment and structure refinement statistics are summarized in Supplementary Table 1.

UV-Vis spectroscopy

Samples of *Ph*Dph2 (50 μM), with and without dithionite, were prepared anaerobically in 150 mM NaCl and 200 mM Tris-HCl at pH 7.4. The sample treated with dithionite was allowed to incubate for 30 min after adding the reducing agent at a final concentration of 0.5 mM. The samples were sealed in a Quartz cell (100 μl each) before taking out from the anaerobic chamber. UV-Vis spectra were obtained on a Cary 50 Bio UV-Visible spectrophotometer (Varian), scanning from 200 nm to 800 nm. The baseline was corrected with the buffer used to prepare the samples.

EPR spectroscopy

ESR spectra were recorded at ACERT on a Bruker EMX spectrometer at a frequency of 9.24 GHz under standard conditions in 4 mm ID quartz tubes. The tubes were filled with *Ph*Dph2 solutions in an oxygen-free atmosphere and sealed under vacuum at 77 K. ESR measurements at 5–50 K were carried out using a liquid helium cryostat, ESR-10 (Oxford Instruments Ltd, England). The spectrometer settings were: modulation frequency 100 kHz, modulation amplitude 8 G, microwave power 0.63 mW.

Mössbauer spectroscopy

Mössbauer spectra were recorded on a spectrometer from WEB research (Edina, MN) operating in the constant acceleration mode in transmission geometry. Spectra were recorded with the temperature of the sample maintained at 4.2 K using a SVT-400 cryostat from Janis (Wilmington, MA) in an externally applied magnetic field of 53 mT oriented parallel to the γ-beam. The quoted isomer shifts are relative to the centroid of the spectrum of a foil of α-Fe metal at room temperature. Data analysis was performed using the program WMOSS from WEB research.

Supplementary Material

Refer to Web version on PubMed Central for supplementary material.

Acknowledgements

We thank Leslie Kinsland for assistance with manuscript preparation, the Dreyfus Foundation for a New Faculty Award to H.L., NIH/NIGMS R01GM088276 to H.L. and S.E.E., and NIH/NCRR P41-RR016292 for the ACERT Center Grant to J.F. This work is based upon research conducted at the APS on the Northeastern Collaborative Access Team beamlines, which are supported by award RR-15301 from the National Center for Research Resources at the National Institutes of Health. Use of the APS is supported by the U.S. Department of Energy, Office of Basic Energy Sciences, under Contract No. DE-AC02-06CH11357.

REFERENCES

1. 2005http://www.cdc.gov/ncidod/DBMD/diseaseinfo/diptheria_t.htm
2. Collier RJ. Understanding the mode of action of diphtheria toxin: a perspective on progress during the 20th century. Toxicon. 2001; 39:1793–1803. [PubMed: 11595641]
3. Liu S, Milne GT, Kuremsky JG, Fink GR, Leppla SH. Identification of the proteins required for biosynthesis of diphthamide, the target of bacterial ADP-ribosylating toxins on translation elongation factor 2. Mol. Cell. Biol. 2004; 24:9487–9497. [PubMed: 15485916]
4. Gomez-Lorenzo MG, Spahn CMT, Agrawal RK, Grassucci RA, Penczek P, Chakraburtty K, et al. Three-dimensional cryo-electron microscopy localization of EF2 in the *Saccharomyces cerevisiae* 80S ribosome at 17.5 Å resolution. EMBO J. 2000; 19:2710–2718. [PubMed: 10835368]
5. Ortiz PA, Ulloque R, Kihara GK, Zheng H, Kinzy TG. Translation elongation factor 2 anticodon mimicry domain mutants affect fidelity and diphtheria toxin resistance. J. Biol. Chem. 2006; 281:32639–32648. [PubMed: 16950777]
6. Walsh, CT. Posttranslational modifications of proteins: Expanding nature's inventory. Roberts and Company Publishers; Englewood, Colorado: 2006.
7. Moehring JM, Moehring TJ, Danley DE. Posttranslational modification of elongation factor 2 in diphtheriatoxin-resistant mutants of CHO-K1 cells. Proc. Natl. Acad. Sci. USA. 1980; 77:1010–1014. [PubMed: 6928655]
8. Moehring TJ, Danley DE, Moehring JM. In vitro biosynthesis of diphthamide, studied with mutant Chinese hamster ovary cells resistant to diphtheria toxin. Mol. Cell. Biol. 1984; 4:642–650. [PubMed: 6717439]
9. Chen JY, Bodley JW, Livingston DM. Diphtheria toxin-resistant mutants of *Saccharomyces cerevisiae*. Mol. Cell. Biol. 1985; 5:3357–3360. [PubMed: 3915773]
10. Mattheakis L, Shen W, Collier R. DPH5, a methyltransferase gene required for diphthamide biosynthesis in *Saccharomyces cerevisiae*. Mol. Cell. Biol. 1992; 12:4026–4037. [PubMed: 1508200]
11. Mattheakis LC, Sor F, Collier RJ. Diphthamide synthesis in *Saccharomyces cerevisiae*: structure of the DPH2 gene. Gene. 1993; 132:149. [PubMed: 8406038]

12. Phillips NJ, Ziegler MR, Deaven LL. A cDNA from the ovarian cancer critical region of deletion on chromosome 17p13.3. Cancer Lett. 1996; 102:85. [PubMed: 8603384]
13. Schultz DC, Balasara BR, Testa JR, Godwin AK. Cloning and localization of a human diphthamide biosynthesis-like protein-2 gene,DPH2L2. Genomics. 1998; 52:186. [PubMed: 9782084]
14. Altschul SF, Gish W, Miller W, Myers EW, Lipman DJ. Basic local alignment search tool. J. Mol. Biol. 1990; 215:403–10. [PubMed: 2231712]
15. Frey PA, Hegeman AD, Ruzicka FJ. The radical SAM superfamily. Crit. Rev. Biochem. Mol. Biol. 2008; 43:63–88. [PubMed: 18307109]
16. Sakuraba H, Tsuge H, Yoneda K, Katunuma N, Ohshima T. Crystal structure of the NAD biosynthetic enzyme quinolinate synthase. J. Biol. Chem. 2005; 280:26645–26648. [PubMed: 15937336]
17. Sofia HJ, Chen G, Hetzler BG, Reyes-Spindola JF, Miller NE. Radical SAM, a novel protein superfamily linking unresolved steps in familiar biosynthetic pathways with radical mechanisms: functional characterization using new analysis and information visualization methods. Nucl. Acids Res. 2001; 29:1097–1106. [PubMed: 11222759]
18. Chatterjee A, Li Y, Zhang Y, Grove TL, Lee M, Krebs C, et al. Reconstitution of ThiC in thiamine pyrimidine biosynthesis expands the radical SAM superfamily. Nat. Chem. Biol. 2008; 4:758–765. [PubMed: 18953358]
19. Makinen GB, Wells MW. Sigel H, Sigel A. ENDOR, EPR and electron spin echo for probing coordination spheres. 1987:129–204.
20. Lieder KW, Booker S, Ruzicka FJ, Beinert H, Reed GH, Frey PA. S-adenosylmethionine-dependent reduction of lysine 2,3-aminomutase and observation of the catalytically functional iron-sulfur centers by electron paramagnetic resonance. Biochemistry. 1998; 37:2578–2585. [PubMed: 9485408]
21. Walsby CJ, Hong W, Broderick WE, Cheek J, Ortillo D, Broderick JB, et al. Electron-nuclear double resonance spectroscopic evidence that S-adenosylmethionine binds in contact with the catalytically active $[4Fe\text{-}4S]^{+}$ cluster of pyruvate formate-lyase activating enzyme. J. Am. Chem. Soc. 2002; 124:3143–3151. [PubMed: 11902903]
22. Cicchillo RM, Tu L, Stromberg JA, Hoffart LM, Krebs C, Booker SJ. *Escherichia coli* quinolinate synthetase does indeed harbor a [4Fe-4S] cluster. J. Am. Chem. Soc. 2005; 127:7310–7311. [PubMed: 15898769]
23. Saunders AH, Griffiths AE, Lee K-H, Cicchillo RM, Tu L, Stromberg JA, et al. Characterization of quinolinate synthases from *Escherichia coli*, *Mycobacterium tuberculosis*, and *Pyrococcus horikoshii* indicates that [4Fe-4S] clusters are common cofactors throughout this cass of enzymes. Biochemistry. 2008; 47:10999–11012. [PubMed: 18803397]
24. McGlynn SE, Boyd ES, Shepard EM, Lange RK, Gerlach R, Broderick JB, et al. Identification and characterization of a novel member of the radical AdoMet enzyme superfamily and implications for the biosynthesis of the Hmd hydrogenase active site cofactor. J. Bacteriol. 2010; 192:595–598. [PubMed: 19897660]
25. Berkovitch F, Nicolet Y, Wan JT, Jarrett JT, Drennan CL. Crystal structure of biotin synthase, an *S*-adenosylmethionine-dependent radical enzyme. Science. 2004; 303:76–79. [PubMed: 14704425]
26. Layer G, Moser J, Heinz DW, Jahn D, Schubert W-D. Crystal structure of coproporphyrinogen III oxidase reveals cofactor geometry of Radical SAM enzymes. EMBO J. 2003; 22:6214–6224. [PubMed: 14633981]
27. Lepore BW, Ruzicka FJ, Frey PA, Ringe D. The x-ray crystal structure of lysine-2,3-aminomutase from *Clostridium subterminale*. Proc. Natl. Acad. Sci. USA. 2005; 102:13819–13824. [PubMed: 16166264]
28. Hanzelmann P, Schindelin H. Crystal structure of the S-adenosylmethionine-dependent enzyme MoaA and its implications for molybdenum cofactor deficiency in humans. Proc. Natl. Acad. Sci. USA. 2004; 101:12870–12875. [PubMed: 15317939]
29. Vey JL, Yang J, Li M, Broderick WE, Broderick JB, Drennan CL. Structural basis for glycyl radical formation by pyruvate formate-lyase activating enzyme. Proc. Natl. Acad. Sci. USA. 2008; 105:16137–16141. [PubMed: 18852451]

30. Marinoni I, Nonnis S, Monteferrante C, Heathcote P, Hartig E, Bottger LH, et al. Characterization of L-aspartate oxidase and quinolinate synthase from *Bacillus subtilis*. FEBS J. 2008; 275:5090–107. [PubMed: 18959769]
31. Rekittke I, Wiesner J, RoÌ^hrich R, Demmer U, Warkentin E, Xu W, et al. Structure of (E)-4-hydroxy-3-methyl-but-2-enyl diphosphate reductase, the terminal enzyme of the non-mevalonate pathway. J. Am. Chem. Soc. 2008; 130:17206–17207. [PubMed: 19035630]
32. Walsby CJ, Ortillo D, Broderick WE, Broderick JB, Hoffman BM. An anchoring role for FeS clusters: Chelation of the amino acid moiety of S-adenosylmethionine to the unique iron site of the [4Fe-4S] cluster of pyruvate formate-lyase activating enzyme. J. Am. Chem. Soc. 2002; 124:11270–11271. [PubMed: 12236732]
33. Krogan NJ, Cagney G, Yu H, Zhong G, Guo X, Ignatchenko A, et al. Global landscape of protein complexes in the yeast *Saccharomyces cerevisiae*. 2006; 440:637.
34. Gavin A-C, Aloy P, Grandi P, Krause R, Boesche M, Marzioch M, et al. Proteome survey reveals modularity of the yeast cell machinery. Nature. 2006; 440:631–636. [PubMed: 16429126]
35. Collins SR, Kemmeren P, Zhao X-C, Greenblatt JF, Spencer F, Holstege FCP, et al. Toward a comprehensive atlas of the physical Interactome of *Saccharomyces cerevisiae*. Mol. Cell. Proteomics. 2007; 6:439–450. [PubMed: 17200106]
36. Proudfoot M, Sanders SA, Singer A, Zhang R, Brown G, Binkowski A, et al. Biochemical and structural characterization of a novel family of cystathionine β-synthase domain proteins fused to a Zn ribbon-like domain. J. Mol. Biol. 2008; 375:301–315. [PubMed: 18021800]
37. Johnson DC, Dean DR, Smith AD, Johnson MK. Structure, function, and formation of biological iron-sulfur clusters. Annu. Rev. Biochem. 2005; 74:247–281. [PubMed: 15952888]
38. Lill R, Muhlenhoff U. Maturation of iron-sulfur proteins in eukaryotes: mechanisms, connected processes, and diseases. Annu. Rev. Biochem. 2008; 77:669–700. [PubMed: 18366324]
39. Otwinowski Z, Minor W. Processing of x-ray diffraction data collected in oscillation mode. Methods Enzymol. 1997; 276:307–326.
40. Sheldrick GM. A short history of SHELX. Acta Crystallogr. A. 2008; 64:112–122. [PubMed: 18156677]
41. Collaborative Computational Project-Number 4. The CCP-4 suite: programs for protein crystallography. Acta. Crystallogr. D. 1994; 50:760–763. [PubMed: 15299374]
42. Terwilliger TC. Reciprocal-space solvent flattening. Acta Crystallogr. D Biol. Crystallogr. 1999; 55:1863–1871. [PubMed: 10531484]
43. Terwilliger TC. Maximum-likelihood density modification. Acta Crystallogr. D Biol. Crystallogr. 2000; 56:965–972. [PubMed: 10944333]
44. Emsley P, Cowtan K. Coot: model-building tools for molecular graphics. Acta Crystallogr. D Biol. Crystallogr. 2004; 60:2126–32. [PubMed: 15572765]
45. Murshudov GN, Vagin AA, Dodson EJ. Refinement of macromolecular structures by the maximum-likelihood method. Acta Crystallogr. D Biol. Crystallogr. 1997; 53:240–55. [PubMed: 15299926]
46. Adams PD, Grosse-Kunstleve RW, Hung LW, Ioerger TR, McCoy AJ, Moriarty NW, et al. PHENIX: building new software for automated crystallographic structure determination. Acta Crystallogr. D Biol. Crystallogr. 2002; 58:1948–54. [PubMed: 12393927]
47. Brünger AT, Adams PD, Clore GM, DeLano WL, Gros P, Grosse-Kunstleve RW, et al. Crystallography & NMR system: A new software suite for macromolecular structure determination. Acta Crystallogr. D Biol. Crystallogr. 1998; 54:905–21. [PubMed: 9757107]

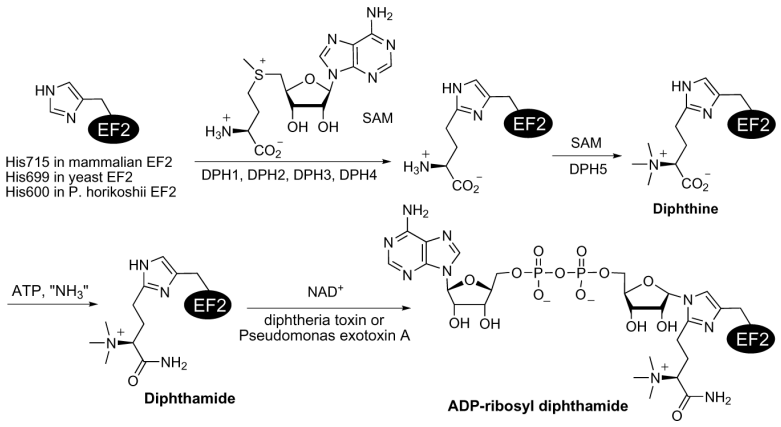

Figure 1.

The structure of diphthamide and its proposed biosynthesis pathway. The diphthamide residue is the target of bacterial ADP-ribosyltransferases, diphtheria toxin and *Pseudomonas* exotoxin A.

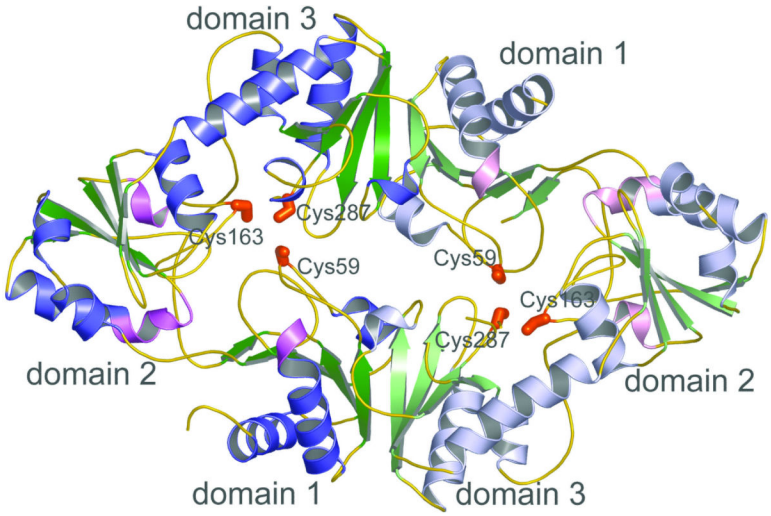

Figure 2.

Structure of *Ph*DPH2 homodimer. The *Ph*Dph2 homodimer is shown in the ribbon diagram with one monomer in dark color and the other in light color. Each monomer is also color by secondary structure. The three conserved cysteine residues for each monomer are shown in the stick representation.

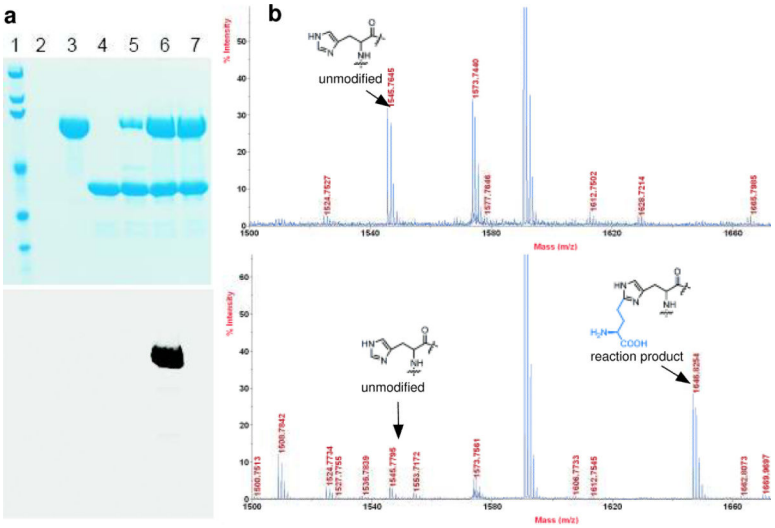

Figure 3.

In vitro reconstitution of *Ph*Dph2 activity. **a**, Activity assay using carboxy-^{14}C SAM. Top panel shows the Coomassie blue-stained gel; bottom panel shows the autoradiography. Lane **1**: Protein standard; **2**: Blank lane; **3**: *Ph*EF2 + SAM, negative control; **4**: *Ph*Dph2 + SAM, negative control; **5**: *Ph*EF2 H600A + *Ph*Dph2 + SAM, negative control; **6**: *Ph*EF2 + *Ph*Dph2 + SAM + dithionite; **7**: *Ph*EF2 + *Ph*Dph2 + SAM, no dithionite, negative control. **b**, The MALDI-MS spectra of *Ph*EF2 unmodified (top) and modified by *Ph*Dph2 in an *in vitro* reaction (bottom).

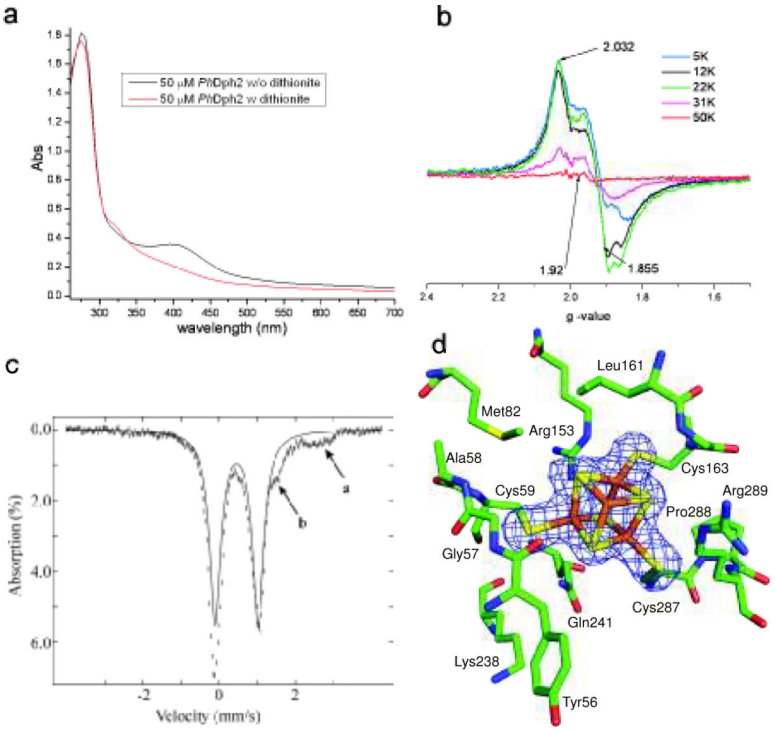

Figure 4.

Spectroscopic characterization of the [4Fe-4S] cluster in *Ph*Dph2. **a**, UV-vis absorption spectra of anaerobically-isolated and dithionite-reduced *Ph*Dph2. **b**, X-band EPR spectra of dithionite-reduced *Ph*Dph2 at different temperature. **c**, 4.2-K/53-mT Mössbauer spectrum of anaerobically-isolated ^{57}Fe-labeled *Ph*Dph2 expressed in *E. coli*. **d**, Structure of *Ph*Dph2 with [4Fe-4S] cluster.

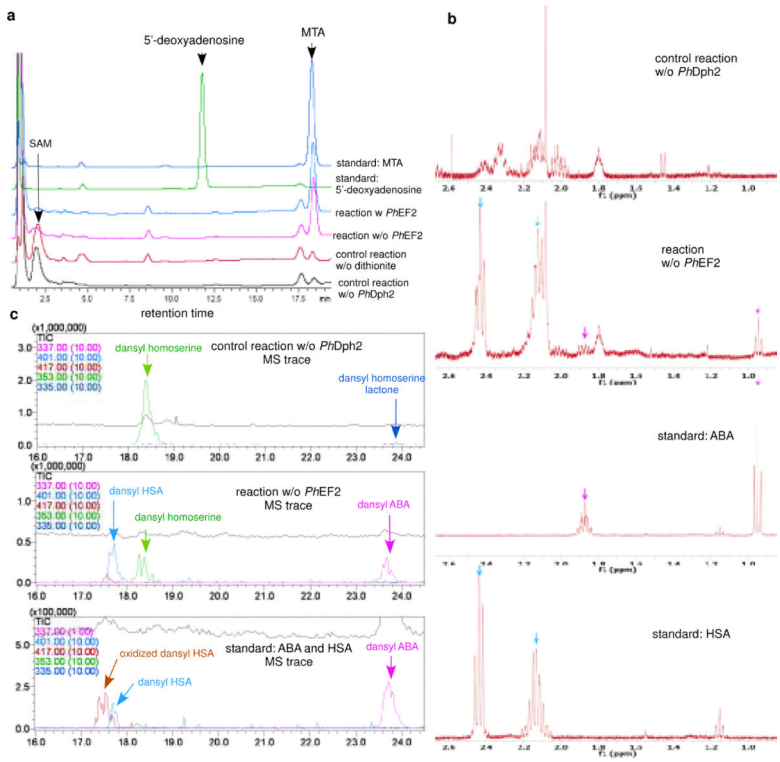

Figure 5.

Identification of SAM-derived small molecule products in *Ph*Dph2-catalyzed reactions. a, HPLC analysis of reaction products suggests *Ph*Dph2 does not form 5′-deoxyadenosine. b, ^{1}H-NMR showing that ABA and HSA formed in the reaction when *Ph*EF2 was not present, but not in control reaction where *Ph*Dph2 was not present. The peaks from HSA and ABA are marked by blue and magenta arrows, respectively. c, Detection of dansylated reaction products by LCMS. The MS traces (total ion counts and ion counts for specific compounds) were shown for the reaction with *Ph*Dph2, control reaction without *Ph*Dph2, and ABA and HSA standards.

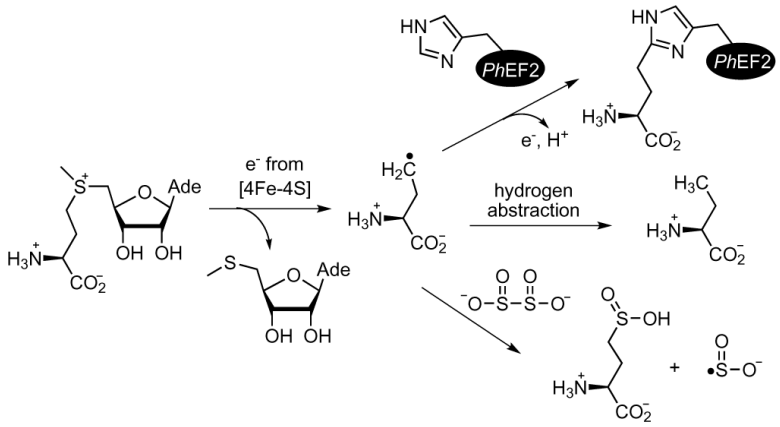

Figure 6.

The proposed reaction mechanism for *Ph*Dph2. The formation of ABA and HSA can be best explained by a 3-amino-3-carboxypropyl radical intermediate. The radical can be generated by electron transfer from the [4Fe-4S] cluster, similar to the generation of 5′-deoxyadenosyl radical in other radical SAM enzymes. In the presence of *Ph*EF2, the radical will react with *Ph*EF2 to form the modified *Ph*EF2 product. In the absence of *Ph*EF2, the radical can either abstract a hydrogen atom to form ABA or be quenched by dithionite to give HSA.